FIR Window and Phase Lead Effects in Repetitive Control for Exoskeleton Tracking

Panya Minyong[1], Phichitphon Chotikunnan[2,*], Rawiphon Chotikunnan[2], Nuntachai Thongpance[2], Yutthana Pititheeraphab[2], Songtham Deewanichsakul[1], Udomsak Jantontapo[1], and Surachat Chantarachit[1]
[1] Mechatronics and Robotics Engineering Established under the Faculty of Technical Education, Rajamangala University of Technology Thanyaburi, Pathum Thani, Thailand
[2] College of Biomedical Engineering, Rangsit University, Pathum Thani, Thailand
Email: panya_m@rmutt.ac.th (P.M.), phichitphon.c@rsu.ac.th (P.C.), rawiphon.c@rsu.ac.th (R.C.), nuntachai.t@rsu.ac.th (N.T.), yutthana.p@rsu.ac.th (Y.P.), songtham_d@rmutt.ac.th (S.D.), udomsak_j@rmutt.ac.th (U.J.), surachat_c@rmutt.ac.th (S.C.)

Manuscript received January 8, 2026; revised March 9, 2026; accepted March 31, 2026
*Corresponding author

***Abstract*—This study investigates a repetitive-control plug-in integrated with a Proportional–Integral–Derivative (PID) controller for a two-degree-of-freedom lower-limb robotic system consisting of hip and knee joints. All experiments were conducted in a MATLAB-based discrete-time simulation using periodic reference trajectories. The proposed plug-in incorporates a Finite-Impulse-Response (FIR) time window and a ring-buffer structure to reuse previously learned control signals, while a phase-lead compensation term is introduced to improve tracking response. System performance was evaluated using the Root Mean Square Error (RMSE) of joint angle tracking during iterative learning cycles and under steady-state conditions. A systematic analysis was performed by varying the lead compensation parameter (rcLead = 0, 2, 4, and 6) and the FIR window length (winLen = 3, 5, and 7), with an additional steady-state evaluation at winLen = 9. Simulation results show that the controller rapidly reduces tracking errors and achieves stable convergence across all tested configurations. The best performance was obtained with rcLead = 2 and winLen = 5, which yielded the lowest steady-state RMSE values of 0.014510 degrees for the hip joint and 0.004741 degrees for the knee joint, while also providing the fastest practical convergence. Larger lead values increased residual tracking errors, whereas excessively short or long window lengths either amplified noise or introduced additional response delays. The results demonstrate that combining moderate phase-lead compensation with an intermediate FIR window length provides an effective and computationally efficient approach for periodic trajectory tracking in multi-joint robotic systems. Future work will focus on experimental validation using a physical platform, evaluation under more diverse motion conditions, and the development of adaptive strategies for automatic parameter tuning.**

***Index Terms*—Finite-Impulse-Response (FIR) window, lower-limb exoskeleton, phase compensation, Proportional–Integral–Derivative (PID), Q-filter, repetitive control, trajectory tracking**

I. Introduction

Lower-limb exoskeletons are increasingly employed for rehabilitation and mobility enhancement, particularly in applications involving gait assistance and neurological recovery. Recent studies report significant progress in mechanical design, actuation mechanisms, and cooperative control strategies for wearable robotic systems. However, accurate cyclic tracking of hip and knee motion remains challenging due to model uncertainties, transmission elasticity, and external disturbances that may generate residual steady-state errors during repetitive motion tasks [1–3]. Additional investigations indicate that actuator compliance, torque saturation, and mechanical transmission characteristics can limit the achievable control bandwidth and consequently reduce trajectory tracking accuracy in wearable robotic platforms [4–6]. These challenges are especially critical in rehabilitation systems where precise and stable joint motion is required to ensure safe human–robot interaction and effective therapeutic assistance.

Proportional–Integral–Derivative (PID) controllers are widely used in wearable robotic systems because of their structural simplicity, robustness, and ease of parameter tuning [7, 8]. Despite these advantages, conventional PID controllers may experience performance limitations when tracking periodic gait trajectories. Phase lag and residual tracking errors frequently occur when actuator nonlinearities, transmission dynamics, and saturation effects are present in the control loop [9, 10]. When cyclic motions are repeated continuously, small tracking errors may accumulate over time, thereby reducing control accuracy and degrading motion assistance performance. These limitations motivate the investigation of learning-based and repetitive control approaches capable of compensating for periodic disturbances and tracking errors in cyclic robotic motions [11, 12].

Repetitive Control (RC), derived from the internal model principle, has been widely studied as an effective strategy for improving tracking performance in periodic motion systems. By incorporating a memory mechanism of the periodic reference signal into the control loop, repetitive control enables the controller to learn from tracking errors in previous cycles and gradually reduce repetitive disturbances over time [13, 14]. In discrete-time implementations, the stability and convergence characteristics of repetitive controllers are strongly influenced by the design of the Q-filter and phase-lead

doi: 10.18178/ijeetc.15.3.221-232

compensation components. These elements are typically introduced to attenuate high-frequency disturbances while compensating for phase delays caused by plant dynamics and digital sampling processes [15, 16].

Recent studies on iterative learning control and repetitive control demonstrate that cyclic tracking performance can be significantly improved by exploiting learning mechanisms across repeated motion cycles [17, 18]. Advanced learning-based control approaches have also been proposed to enhance robustness against model uncertainties and delay variations through adaptive and model-based designs [19, 20]. Such learning-based frameworks allow controllers to progressively refine control inputs based on previously observed tracking performance, thereby improving accuracy in repetitive trajectory tracking tasks.

Among the key components of repetitive control design, the Q-filter plays a critical role in determining the convergence speed and stability of the learning process. FIR windowed Q-filters, including rectangular and Hann window structures, have been investigated for their ability to regulate the frequency response of the repetitive controller while limiting memory usage and providing moderate phase-lead compensation to improve convergence characteristics [21–23]. Proper selection of Q-filter bandwidth and phase-lead parameters is therefore essential for achieving stable and efficient learning behavior in cyclic motion control systems.

In wearable robotic systems such as lower-limb exoskeletons, cyclic tracking performance is influenced not only by controller design but also by actuator compliance, human–robot interaction dynamics, and sensing uncertainty [24, 25]. Previous studies indicate that appropriate bandwidth limitation, moderate phase-lead compensation, and carefully selected learning gains can significantly improve convergence speed while maintaining closed-loop stability during cyclic motion control tasks [26, 27]. These design considerations are particularly important in exoskeleton systems where safe and stable assistance must be maintained despite variations in human biomechanics and walking cadence.

Adaptive and learning-based control strategies have therefore been increasingly integrated into mechatronic and wearable robotic systems to improve cyclic motion performance under uncertain operating conditions and slow cadence variations [28, 29]. These approaches include gain-scheduled PID control, compliant actuator modeling, and synergy-based actuation mechanisms designed to improve adaptability in nonlinear human–robot interaction environments [30–32]. In addition, data-driven identification and model-based parameter estimation techniques have been explored to enhance control accuracy and robustness in human–exoskeleton systems [31, 33].

In this context, repetitive control offers a practical advantage for wearable robotic applications because it can compensate for periodic tracking errors within a relatively simple control architecture. By synchronizing feedforward reference trajectories with the dynamic characteristics of the robotic system, repetitive controllers can improve trajectory tracking accuracy while reducing energy consumption during repeated gait cycles [29, 34]. These characteristics make repetitive control particularly suitable for lower-limb exoskeleton systems where stable and accurate cyclic motion assistance is required for rehabilitation and mobility support [34, 35].

Despite these advances, the influence of repetitive control parameter design, particularly the selection of FIR-based Q-filter window length and discrete phase-lead compensation, has not been systematically investigated for lower-limb exoskeleton tracking applications. In many existing studies, repetitive control parameters are selected empirically without detailed analysis of how Q-filter structure and phase compensation influence convergence behavior, tracking accuracy, and stability in wearable robotic systems. A systematic parameter analysis is therefore necessary to better understand how FIR Q-filter configuration affects cyclic motion control performance in wearable robotics.

A. Objective and Contributions

This study investigates the combined use of proportional–integral–derivative control and repetitive control for cyclic trajectory tracking in a planar two-degree-of-freedom hip–knee exoskeleton system. The analysis focuses on two key discrete-time repetitive control design parameters, namely the window length of the FIR-based Q-filter and the use of discrete phase-lead compensation. A MATLAB-based simulation framework is developed to evaluate cyclic tracking performance under realistic actuator conditions, including gravitational effects, viscous damping, actuator saturation, and anti-windup protection. System performance is assessed using root mean square error and phase delay under sinusoidal gait trajectory inputs.

The primary contribution of this work is the development of a reproducible simulation framework that isolates the influence of FIR Q-filter window length and phase-lead compensation on cyclic tracking performance in wearable robotic systems. Simulation results show that moderate phase-lead compensation combined with a medium-length FIR window significantly reduces both transient and steady-state tracking errors. Specifically, a two-sample phase-lead compensation together with a five-sample FIR Q-filter achieves steady-state root mean square error values of 0.0145° for the hip joint and 0.0047° for the knee joint under actuator saturation conditions, demonstrating improved cyclic tracking performance in the proposed exoskeleton control framework.

II. Literature Review

A. Lower-Limb Exoskeletons: Structures and Control

Exoskeletons designed for rehabilitation and assistance of the lower limbs employ actuation technologies including electric, pneumatic, and series-elastic systems [1–3]. Multimodal sensing systems, comprising inertial and force sensors, enhance perception and control capabilities in wearable robotic platforms [4–6]. Recent advancements have highlighted sensor fusion, adaptive mechanical architectures, and human–robot interaction modeling to improve motion stability, safety, and user comfort in wearable robotic systems [36–38].

Gravity, damping coefficients, and transmission

elasticity are prevalent in multi-link dynamic models. These factors introduce phase lag, reduce effective control bandwidth, and complicate precise cyclic trajectory tracking in multi-joint wearable systems [39, 40]. Upper-limb systems affected by actuator saturation and backlash exhibit similar dynamic limitations [12]. The integration of variable stiffness actuators and torque estimation using unscented Kalman filtering enables accurate identification of gait phases [39]. Cable-driven exosuits employ postural and dynamic synergies to reduce the number of actuators while maintaining kinematic compatibility [40, 41].

Accurate cyclic tracking in wearable joints therefore requires compensation for phase lag and periodic disturbances caused by compliant actuation and system dynamics. These challenges motivate the development of control strategies designed to reduce periodic tracking errors in cyclic gait motions.

B. PID Servo Loops and Practical Enhancements in Wearable Robotics

PID control is widely used in wearable robotic systems due to its simple architecture and computational efficiency [7–9]. It provides reliable trajectory tracking across various assistive and rehabilitation platforms [10–12]. Anti-windup mechanisms effectively manage actuator saturation and prevent integrator drift [10], while gain-scheduled and adaptive approaches improve controller performance under varying operating conditions [28, 29]. Observer-based feedback and torque estimation techniques can further reduce tracking errors without requiring full plant identification [34].

Despite these advantages, conventional PID control structures are not inherently designed to eliminate periodic disturbances that repeatedly occur in cyclic gait trajectories. Consequently, classical PID controllers may exhibit residual steady-state errors when identical disturbances appear in successive motion cycles.

C. Repetitive Control and Q-Filter Design in Discrete Time

Repetitive control employs an internal model of the task period to compensate for periodic tracking errors [13–15]. The effectiveness of discrete-time repetitive control depends strongly on the characteristics of the Q-filter and the applied phase compensation mechanisms [16–18]. FIR-based Q-filters, including Hann and rectangular window configurations, reduce memory usage and improve noise robustness while providing slight phase-lead adjustments [19–22].

The selection of Q-filter bandwidth and filter window length significantly affects convergence behavior, noise attenuation, and tracking accuracy in repetitive control systems. The window length influences convergence speed and noise rejection capability, whereas excessive phase lead may degrade steady-state tracking accuracy [23–25]. Therefore, appropriate parameter selection is essential to ensure stable convergence and effective periodic error suppression.

D. Learning for Periodic Motion: ILC/RC vs. Neural Policy Approaches

Iterative learning control (ILC) and repetitive control, both derived from the internal model principle, aim to reduce tracking error across successive motion cycles [13–15]. These approaches have demonstrated progressive improvements in mechatronic and wearable robotic systems when gait cadence is constant or varies slowly [28, 30, 31].

Neural locomotion controllers based on central pattern generators and deep learning techniques have enabled adaptive policy generation and scalable gait modulation for rehabilitation applications [32, 35]. These data-driven approaches allow adaptive behavior but generally require extensive training datasets and considerable computational resources.

Although neural policies demonstrate adaptability, they cannot inherently eliminate deterministic periodic tracking errors unless explicitly trained for those patterns. In contrast, repetitive control provides a computationally efficient online strategy capable of mitigating periodic residual errors under constant or slowly varying cadence within a conventional servo control architecture [13–15].

E. Metrics and Reporting for Cyclic Tracking

The performance of wearable exoskeleton controllers is commonly evaluated for each motion cycle using metrics such as root mean square error, mean absolute error, and phase delay [1, 3, 5]. These indices are widely applied in studies assessing dynamic responsiveness and kinematic tracking accuracy in robotic rehabilitation systems [6, 39, 40].

These evaluation metrics enable systematic comparison of cyclic tracking performance and convergence behavior among different controller architectures. In repetitive control studies, RMSE and phase delay are commonly used to evaluate steady-state tracking accuracy and dynamic responsiveness under periodic reference trajectories [22–27].

F. Research Gap and Contribution of This Study

Despite previous advances in PID tuning, adaptive feedback control, and learning-based motion strategies, limited research has systematically investigated the combined influence of FIR Q-filter window length and discrete phase-lead compensation on cyclic tracking performance in wearable exoskeleton systems. Most existing studies select repetitive control parameters empirically without performing systematic parameter exploration or analyzing their influence on convergence speed, tracking accuracy, and robustness.

To address this limitation, the present study investigates the combined effects of FIR Q-filter window length and discrete phase-lead compensation on cyclic tracking performance in a planar two-degree-of-freedom hip–knee exoskeleton model. A MATLAB-based simulation framework is developed that incorporates gravitational load, viscous damping, actuator saturation, and anti-windup protection to enable systematic parameter analysis. Using sinusoidal gait trajectories, the study evaluates how controlled variations in Q-filter length and phase lead influence tracking error, convergence stability, and phase delay characteristics in repetitive control-based wearable

robotic systems.

III. Research Method

This section provides a detailed description of the technique employed in this work, which consists of three primary components, plant and actuation modeling, control system architecture design, and iterative control design. The discrete-time MATLAB implementation satisfies each parameter definition and modeling assumption. The joint angles are determined relative to the horizontal axis in accordance with the gravitational framework of the simulation model.

A. Plant and Actuation Model

The planar Two-Degree-of-Freedom (2-DoF) lower-limb exoskeleton robotic system considered in this work is intended to mimic the sagittal-plane hip and knee motion that occurs during human locomotion. Fig. 1 shows the system coordinate definition and kinematic arrangement.

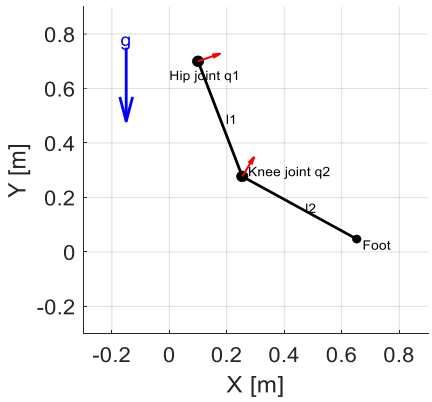

Fig. 1. Two-link planar lower-limb exoskeleton model with hip and knee joints, shaft-side damping, and gravity direction.

The construction consists of two stiff links that are joined by revolute joints. The hip and knee joint angles are indicated by q_1 and q_2, respectively. The definition of the generalized coordinate vector is $\mathbf{q} = [q_1, q_2]^T \in \mathbb{R}^2$.

The Euler–Lagrange approach is used to generate the equations of motion for a two-link manipulator as indicated in Eq. (1):

$$\mathbf{M}(\mathbf{q})\ddot{\mathbf{q}} + \mathbf{C}(\mathbf{q}, \dot{\mathbf{q}})\dot{\mathbf{q}} + \mathbf{G}(\mathbf{q}) = \mathbf{T}_l \quad (1)$$

where $\mathbf{T}_l \in \mathbb{R}^2$ denotes the load-side joint torque vector, $\dot{\mathbf{q}}$ and $\ddot{\mathbf{q}}$ in τ_{sh} are taken at $k-1$, $G(q)$ denotes gravity, $C(q, \dot{q})$ is the Coriolis/centrifugal matrix and $M(q) \in \mathbb{R}^{2\times 2}$ is the inertia matrix.

The model isolates the shaft reaction torque from the total actuator command in order to accurately represent actuator dynamics. The shaft reaction torque is modeled as Eq. (2);

$$\tau_{\text{sh}}[k] = J_m\ddot{\mathbf{q}}[k-1] + B_s\dot{\mathbf{q}}[k-1] \quad (2)$$

where B_s is the shaft viscous damping coefficient and J_m represents the equivalent motor inertia.

The load-side torque exerted on the links is given by Eq. (3):

$$\mathbf{T}_l[k] = \boldsymbol{\tau}[k] - \tau_{\text{sh}}[k] \quad (3)$$

where $\boldsymbol{\tau}[k]$ is the actuator torque command. To avoid integrator windup, the integral term in the controller is frozen once the unsaturated torque surpasses the $|\tau_i| \leq \tau_{max}$ constraint on each joint torque.

Substituting Eq. (2) and Eq. (3) into Eq. (1) yields the actuator-side dynamics:

$$\boldsymbol{\tau} = (\mathbf{M}(\mathbf{q}) + J_m\mathbf{I})\ddot{\mathbf{q}} + \mathbf{C}(\mathbf{q}, \dot{\mathbf{q}})\dot{\mathbf{q}} + \mathbf{G}(\mathbf{q}) + B_s\dot{\mathbf{q}} \quad (4)$$

In discrete time, $\dot{\mathbf{q}}$ and $\ddot{\mathbf{q}}$ in τ_{sh} are evaluated at $k-1$ to avoid algebraic loops at a sampling period of $T_s = 1$ ms; sensitivity to this one-step delay is reported in the supplement. Here, $\mathbf{M}(\mathbf{q})$ denotes the link-side inertia matrix (motor inertia excluded), and the actuator-side inertia is defined as $\widetilde{\mathbf{M}}(\mathbf{q}) = \mathbf{M}(\mathbf{q}) + J_m\mathbf{I}$. The shaft damping is modeled as $B_s\mathbf{I}\,\dot{\mathbf{q}}$, applied equally to both joints.

The matrices $\mathbf{M}(\mathbf{q}), \mathbf{C}(\mathbf{q}, \dot{\mathbf{q}})$, and $\mathbf{G}(\mathbf{q})$ are defined component-wise as:

$$M_{11} = I_1 + m_1 d_1^2 + I_2 + m_2(l_1^2 + d_2^2 + 2l_1 d_2 \cos\, q_2)$$
$$M_{12} = I_2 + m_2(d_2^2 + l_1 d_2 \cos\, q_2)$$
$$M_{21} = M_{12}$$
$$M_{22} = I_2 + m_2 d_2^2$$
$$C_{11} = -m_2 l_1 d_2 \sin\, q_2\, \dot{q}_2$$
$$C_{12} = -m_2 l_1 d_2 \sin\, q_2\, (\dot{q}_1 + \dot{q}_2)$$
$$C_{21} = m_2 l_1 d_2 \sin\, q_2\, \dot{q}_1$$
$$C_{22} = 0$$
$$G_1 = (m_1 d_1 + m_2 l_1) g \sin\, q_1 + m_2 d_2 g \sin\,(q_1 + q_2)$$
$$G_2 = m_2 d_2 g \sin\,(q_1 + q_2)$$

All equations were implemented in MATLAB to compute joint torques at each simulation step, ensuring the reproducibility of the exoskeleton dynamics.

Table I summarizes the physical and dynamic parameters used in the simulations.

TABLE I: Physical and Dynamic Parameters of the Two-Link Exoskeleton Model

Parameter	Description	Value	Unit
l_1	Length of link 1 (thigh)	0.45	m
l_2	Length of link 2 (shank)	0.46	m
d_1	Distance from hip joint to COM of link 1	0.19	m
d_2	Distance from knee joint to COM of link 2	0.20	m
m_1	Mass of link 1	2.0	kg
m_2	Mass of link 2	1.5	kg
I_1	Inertia of link 1 about COM	0.034	kg·m²
I_2	Inertia of link 2 about COM	0.027	kg·m²
g	Gravitational acceleration	9.80665	m/s²
J_m	Equivalent motor inertia	0.010	kg·m²
B_s	Shaft damping coefficient	0.080	N·m·s/rad
$\tau_{\max}$	Maximum joint torque	60	N·m

B. Control Architecture

To accomplish accurate trajectory tracking under cyclic references, the suggested control architecture combines a parallel repetitive control loop with a traditional discrete-time PID controller. While the repetitive control component gradually learns and eliminates periodic tracking faults over several cycles, the PID controller provides baseline stability and disturbance rejection.

For each joint, the PID control law is defined as Eq. (5):

$$\tau_{\text{PID}}[k] = K_p \mathbf{e}[k] + K_i T_s \sum_{i=0}^{k} \mathbf{e}[i] + K_d \frac{\mathbf{e}[k]-\mathbf{e}[k-1]}{T_s} \quad (5)$$

where K_p, K_i, and K_d denote proportional, integral, and derivative gains respectively, T_s is the sampling period, and $e[k] = \mathbf{q}_{\text{ref}}[k] - \mathbf{q}[k]$ represents the tracking error. During actuator saturation, the integral component is suspended to execute anti-windup measures.

For repetitive tasks, a repetitive control loop is implemented in parallel to enhance tracking performance. The repetitive control algorithm uses information from previous cycles to adjust future control actions while retaining past control and error signals. The repetitive control law is expressed as Eq. (6):

$$\boldsymbol{\tau}_{\text{RC}}[k] = Q(z)\boldsymbol{\tau}_{\text{RC}}[k-N] + G(z)\mathbf{e}[k-N] \quad (6)$$

where $G(z)$ is the learning gain, N is the number of samples per reference period, and $Q(z)$ is a FIR Q-filter that governs learning behavior and ensures stability. The total actuator torque applied to the system is given by Eq. (7):

$$\boldsymbol{\tau}[k] = \text{sat}(\boldsymbol{\tau}_{\text{PID}}[k] + \boldsymbol{\tau}_{\text{RC}}[k]) \quad (7)$$

where sat(·) indicates element-wise saturation.

Table II lists the fixed PID gains used in all simulations. The overall control structure integrating PID and repetitive control is illustrated in Fig. 2 and Fig. 3.

TABLE II: PID CONTROLLER PARAMETERS FOR HIP AND KNEE JOINTS

Joint	K_p	K_i	K_d
Hip (q_1)	120	45	20
Knee (q_2)	50	10	10

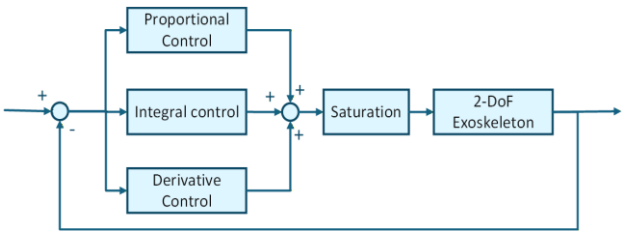

Fig. 2. PID structure for 2-DoF exoskeleton.

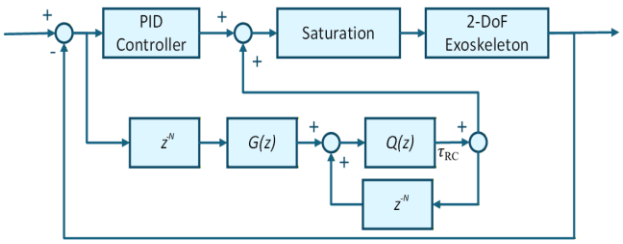

Fig. 3. Control architecture of the PID–repetitive controller for 2-DoF exoskeleton.

As shown in Fig. 2, the baseline PID control architecture for the 2-DoF hip–knee exoskeleton is presented. The desired joint trajectory $\mathbf{q}_{\text{ref}}[k]$ is compared with the measured joint position $\mathbf{q}[k]$ to generate the tracking error $\mathbf{e}[k]$. The PID controller, consisting of proportional, integral, and derivative components, produces the control torque $\tau_{\text{PID}}[k]$according to Eq. (5). The resulting control signal passes through a saturation block representing actuator torque limitations before being applied to the exoskeleton dynamics, while the measured output is fed back to close the control loop.

As illustrated in Fig. 3, the proposed control architecture integrates a repetitive control loop in parallel with the PID controller. The repetitive controller generates an additional torque $\boldsymbol{\tau}_{\text{RC}}[k]$ based on the delayed error $\mathbf{e}[k-N]$ and the previous repetitive control signal $\boldsymbol{\tau}_{\text{RC}}[k-N]$, as defined in Eq. (6). The delay operator z^{-N} represents one period of the cyclic motion, while the FIR Q-filter $Q(z)$ regulates the learning stability. The repetitive control signal is added to the PID output before the saturation block to form the total actuator torque in Eq. (7), enabling progressive reduction of periodic tracking errors across successive cycles.

C. Repetitive Control Design and Parameters

The repetitive control architecture follows the internal model concept allowing the system to eliminate periodic disturbances and achieve near-zero steady-state error. The number of samples per interval for a reference frequency $f_{ref,i}$ is calculated as Eq. (8):

$$N_i = \text{round}(\frac{f_s}{f_{\text{ref},i}}) \quad (8)$$

where f_s is the sampling frequency.

For each joint, a ring buffer is employed to store historical control inputs and tracking errors from the previous cycle. The discrete-time repetitive control update rule is expressed as Eq. (9):

$$\tau_{\text{RC}}[k] = \sum_{n=0}^{L-1} w[n]\, \tau_{\text{RC}}[k - N_i + \text{rcLead} - n] + \gamma_i \sum_{n=0}^{L-1} w[n]\, e_i[k - N_i + \text{rcLead} - n] \quad (9)$$

where $w[n]$ denotes the coefficients of the FIR Q-filter, normalized such that $\sum_{n=0}^{L-1} w[n] = 1$. The parameter rcLead indicates the phase-lead compensation in samples to mitigate the effective system delay, L designates the window length, and γ_i represents the learning gain. The learning gain γ_i has units of torque per angular error, specifically N·m/rad when e_i is expressed in radians, or N·m/degwhen e_i is in degrees.

The Q-filter utilizes a Hann window to ensure unity Direct Current Gain and promote smooth spectral attenuation. The window coefficients are defined as Eq. (10):

$$w[n] = 0.5 - 0.5\cos\left(\frac{2\pi n}{L-1}\right), n = 0,1,\ldots,L-1 \quad (10)$$

The window coefficients defined in (10) are subsequently normalized to guarantee that their sum equals unity.

This study investigates the effects of filter widths L =3,5, and 7 on learning efficacy and noise reduction. An increased L promotes superior smoothing (enhanced attenuation of high-frequency noise) while preserving low-

frequency error components, hence maintaining the Q-filter magnitude close to unity at the fundamental frequency of 0.40 Hz with a sampling frequency of 1 kHz.

Fig. 4 illustrates the complete process of the repetitive control algorithm combined with PID compensation.

The proposed control system was implemented and evaluated using MATLAB in a discrete-time simulation environment. The model represents a two-degree-of-freedom lower-limb robotic system consisting of hip and knee joints. The dynamic behavior of the system was modeled using a standard planar two-link robot model that includes inertia, Coriolis/centrifugal effects, and gravitational torques. In addition, a simplified actuator shaft model including inertia and viscous damping was incorporated to represent motor–joint dynamics.

A discrete-time control loop was implemented with a sampling frequency of 1000 Hz. At each sampling step, the joint tracking error between the reference trajectory and the simulated joint angle was computed. A PID controller generated the baseline control torque, while the repetitive-control plug-in provided an additional correction term to compensate for periodic tracking errors. The combined control signal was subjected to actuator torque saturation limits, and an anti-windup mechanism was applied to prevent integrator accumulation when saturation occurred.

The repetitive-control mechanism was implemented using a time-window FIR Q-filter together with a ring-buffer structure that stores the tracking errors from the previous motion cycle. The stored information was reused in subsequent iterations through the Q-filter and a phase-lead compensation term. The resulting repetitive-control signal was then added to the PID output to improve periodic trajectory tracking performance.

The simulation was executed for multiple learning iterations to analyze the convergence behavior of the repetitive controller. Different combinations of phase-lead compensation (rcLead) and FIR window length (winLen) were evaluated to investigate their influence on convergence speed and steady-state tracking accuracy. For each configuration, the tracking performance of both hip and knee joints was quantified using the RMSE of the joint angle tracking signals.

The simulation parameters used in this study are summarized in Table III.

TABLE III: REPETITIVE CONTROL PARAMETERS FOR SIMULATION

Parameter	Symbol	Value(s)	Description
Sampling frequency	f_s	1000 Hz	Simulation rate
Reference frequency	f_{ref}	0.40 Hz	Fundamental trajectory frequency
Period length	N	2500 samples	Samples per cycle
Learning gain	γ_i	[8 8] N·m/deg	Fixed for hip and knee
Lead compensation	$rcLead$	0, 2, 4, 6	System delay compensation
FIR window length	$winLen$	3, 5, 7, 9	Q-filter shaping
Q-filter type	$Q(z)$	Hann	Smooth spectral roll-off

IV. RESULTS AND DISCUSSION

The selection of rcLead and L strongly influences the convergence characteristics. In the simulations, moderate values such as a two-sample lead and a five-tap window length consistently offer the optimal trade-off between transient responsiveness and steady-state accuracy.

All simulations in this study were conducted using a MATLAB-based environment to evaluate the behavior, performance, and stability of the proposed repetitive-control framework under controlled conditions. The simulation model represents a two-degree-of-freedom lower-limb system consisting of hip and knee joints that follow predefined periodic reference trajectories. This configuration enables a systematic investigation of how different control parameters influence trajectory tracking performance and convergence characteristics.

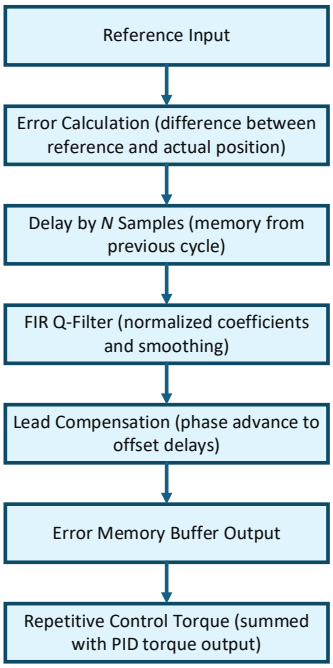

Fig. 4. Flowchart of the repetitive control process integrated with PID compensation.

The primary objective of this section is to analyze the effects of different FIR window lengths (winLen = 3, 5, and 7) and phase-lead compensation values (rcLead = 0, 2, 4, and 6) on the trajectory tracking accuracy of the control system. For each parameter configuration, the controller was evaluated over multiple learning iterations in order to observe the evolution of tracking errors and the convergence behavior of the repetitive-control mechanism. To ensure consistency and comparability across all experiments, the same system dynamics, controller structure, sampling configuration, and reference trajectories were maintained for every simulation scenario. The tracking performance of the system was quantified using the RMSE of the joint angle tracking signals. RMSE values were computed at each iteration to analyze the learning process and were also evaluated under steady-state conditions to assess long-term tracking accuracy.

The analysis focuses on three FIR window lengths

(winLen = 3, 5, and 7), which were selected to investigate the influence of window size on convergence behavior and steady-state tracking performance. By comparing the controller responses across these configurations, the study examines how different window lengths affect the balance between convergence speed, robustness, and tracking accuracy.

Overall, this simulation-based methodology provides a controlled and reproducible framework for evaluating the influence of parameter variations on repetitive-control performance. By isolating the effects of phase-lead compensation and FIR window length, the approach enables clear identification of performance trends and optimal parameter configurations while avoiding external uncertainties typically associated with hardware experimentation.

A. Hip and Knee Joint RMSE Convergence Analysis

The convergence behavior of the hip and knee joint tracking errors under different lead compensation settings and FIR window lengths is presented in Fig. 5 to Fig. 7. Specifically, Fig. 5 illustrate the RMSE convergence of the hip and knee joints with a window length of winLen = 3, Fig. 6 correspond to winLen = 5, and Fig. 7 present the results for winLen = 7. These figures show how the proposed repetitive-control framework progressively reduces trajectory tracking errors across successive learning iterations for different parameter configurations. The corresponding steady-state RMSE values are summarized numerically in Table IV for the hip joint and Table V for the knee joint.

As observed in the convergence plots, both joints exhibit a rapid reduction in RMSE during the initial iterations, indicating that the repetitive control mechanism effectively learns and compensates for periodic tracking errors. For all parameter configurations, the RMSE decreases significantly during the early learning cycles before gradually approaching a steady-state value. This behavior confirms the capability of the proposed control framework to improve trajectory tracking performance through iterative learning.

TABLE IV: HIP RMSE STEADY-STATE MEAN (DEG)

rcLead	winLen 3	winLen 5	winLen 7
0	0.051580	0.092137	0.133217
2	**0.032430**	**0.014510**	0.051571
4	0.109636	0.071053	**0.032419**
6	0.184696	0.147544	0.109627

TABLE V: KNEE RMSE STEADY-STATE MEAN (DEG)

rcLead	winLen 3	winLen 5	winLen 7
0	0.016613	0.032364	0.048594
2	**0.016257**	**0.004741**	0.016598
4	0.046250	0.031250	**0.016241**
6	0.075827	0.061122	0.046244

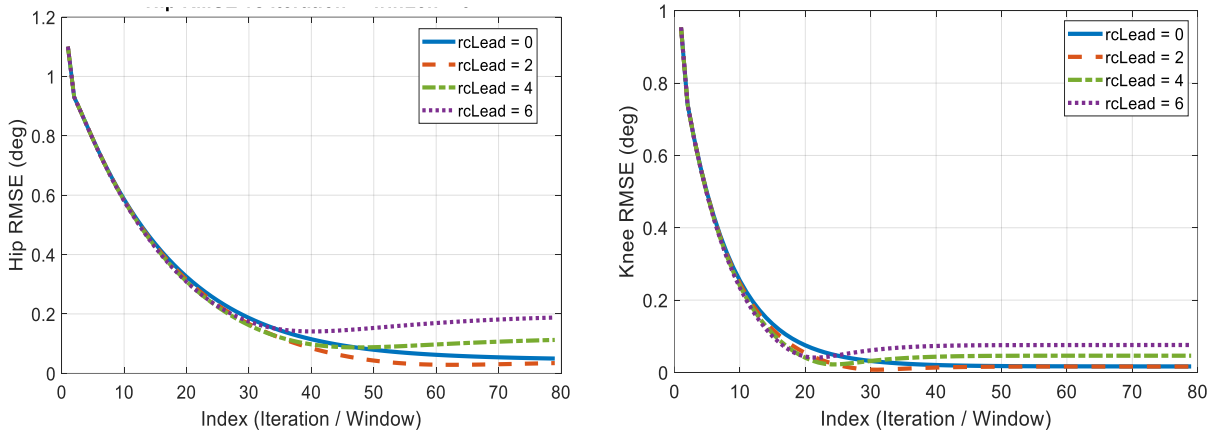

Fig. 5. Across different rcLead settings with winLen 3: (a) Hip joint RMSE convergence and (b) Knee joint RMSE convergence.

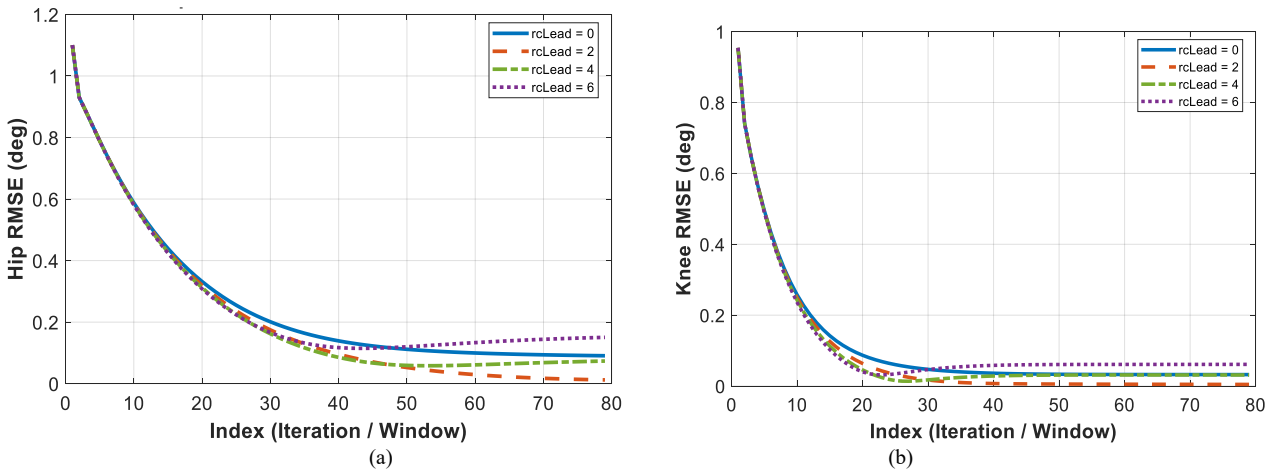

Fig. 6. Across different rcLead settings with winLen 5: (a) Hip joint RMSE convergence and (b) Knee joint RMSE convergence.

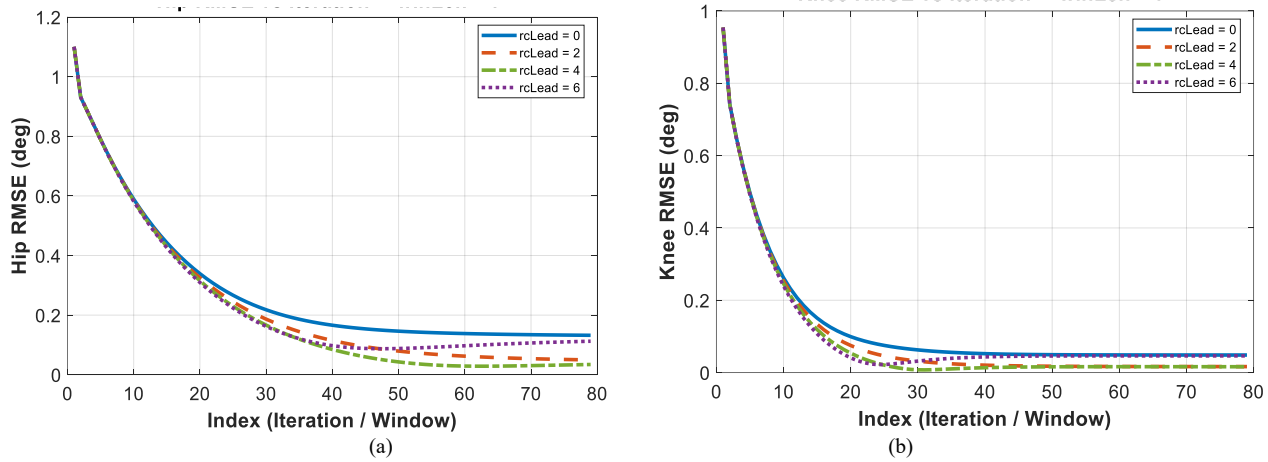

Fig. 7. Across different rcLead settings with winLen 7: (a) Hip joint RMSE convergence and (b) Knee joint RMSE convergence.

The phase-lead compensation parameter (rcLead) has a significant influence on both convergence speed and final tracking accuracy. Across most window-length configurations, rcLead = 2 generally provides the fastest convergence and the lowest steady-state RMSE for both joints. In contrast, larger compensation values such as rcLead = 4 and rcLead = 6 tend to produce slower convergence and larger residual tracking errors. This trend suggests that excessive phase-lead compensation may increase control sensitivity and reduce steady-state tracking precision.

The effect of the FIR Q-filter window length (winLen) can also be observed in the convergence characteristics. Increasing the window length improves the smoothness of the steady-state response due to stronger error averaging, although it slightly slows the initial convergence. Among the evaluated configurations, winLen = 5 provides the most balanced performance between convergence speed and steady-state accuracy. As shown in Table IV, the hip joint achieves its lowest steady-state RMSE of 0.014510 degrees when rcLead = 2 and winLen = 5. Similarly, Table V indicates that the knee joint reaches its minimum steady-state RMSE of 0.004741 degrees under the same parameter configuration.

The consistency of these results across both joints suggests that the interaction between phase-lead compensation and FIR window length follows a similar control mechanism within the repetitive-control framework. Shorter window lengths allow faster adaptation but may increase sensitivity to noise, whereas longer windows introduce additional phase delay that can slow convergence. An intermediate window length therefore provides an effective compromise between responsiveness and stability.

Overall, the results indicate that the parameter combination rcLead = 2 and winLen = 5 provides the most effective configuration for trajectory tracking of both hip and knee joints. This configuration achieves rapid convergence, minimal steady-state error, and stable long-term tracking performance in the simulated exoskeleton control system.

B. Steady-State RMSE Comparison and Parameter Optimization

Fig. 8 illustrate the RMSE convergence behavior of the hip and knee joints under different FIR window lengths when the lead compensation parameter is fixed at rcLead = 2. These figures highlight how the selection of window length influences the convergence characteristics and steady-state tracking accuracy of the control system. The corresponding steady-state RMSE values are summarized numerically in Table VI, which enables a direct comparison of the tracking performance across different parameter configurations.

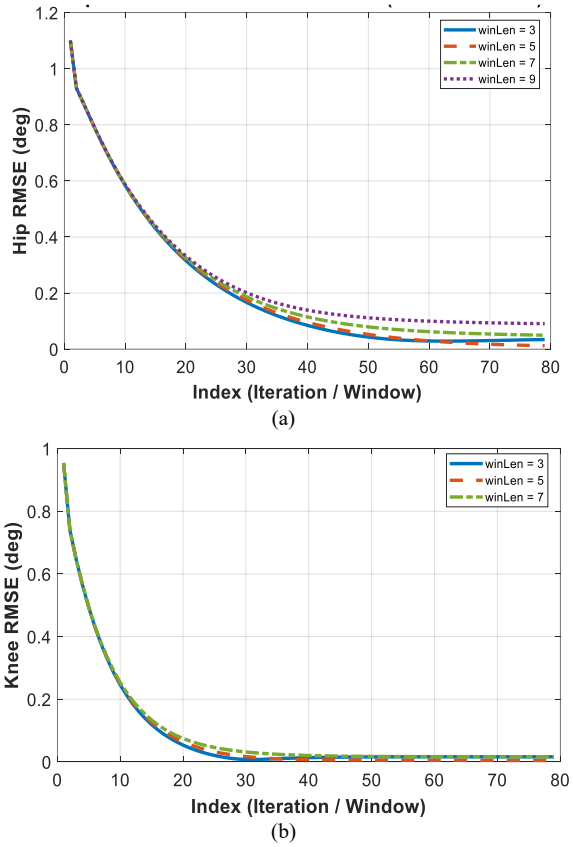

Fig. 8. Across different rcLead settings with winLen 2: (a) Hip Joint RMSE Convergence and (b) Knee Joint RMSE Convergence.

TABLE VI: STEADY-STATE RMSE (DEG) FOR RCLEAD 2

winLen	Hip RMSE	KNEE RMSE
3	0.032430	0.016257
5	**0.014510**	**0.004741**
7	0.051571	0.016598

The results clearly demonstrate that the window length plays a critical role in determining steady-state tracking accuracy. Among the tested configurations (winLen = 3, 5, and 7), winLen = 5 consistently provides the best overall performance for both joints. As shown in Table VI, this configuration achieves the lowest steady-state RMSE values of 0.014510 degrees for the hip joint and 0.004741 degrees for the knee joint. These values are significantly lower than those obtained with other window lengths, indicating that this parameter combination effectively minimizes residual tracking errors.

The convergence behavior observed in Fig. 8(a) and Fig. 8(b) further supports this finding. For all tested window lengths, the RMSE decreases rapidly during the early iterations, demonstrating the ability of the repetitive control framework to progressively learn and compensate for periodic tracking errors. However, differences in the steady-state region become evident as the iteration index increases. The configuration winLen = 5 maintains the lowest RMSE trajectory and achieves the fastest stable convergence for both joints.

C. Best-Case Scenario and Performance Discussion

The final stage of the simulation evaluates the control system using the optimal parameter configuration identified from the previous analysis, namely rcLead = 2 and winLen = 5. This parameter combination was selected based on the steady-state RMSE comparison presented in Table VI, as well as the joint-specific results summarized in Tables IV and V. Under this configuration, the hip joint achieves a steady-state RMSE of 0.014510 degrees, while the knee joint reaches 0.004741 degrees, representing the lowest residual tracking errors among all tested parameter settings.

The time-domain tracking performance under this optimal configuration is illustrated in Fig. 9(a) and Fig. 9(b). These plots demonstrate a close agreement between the reference trajectories and the measured joint angles throughout the simulation period. The tracking signals exhibit minimal phase lag and negligible amplitude deviation, indicating that the control system can accurately reproduce the desired periodic motion. This behavior confirms the effectiveness of the selected parameter combination in maintaining high tracking accuracy while preserving system stability.

Further insight into the system behavior can be observed from the tracking error signals shown in Fig. 9(c). During the initial cycles, both hip and knee tracking errors decrease rapidly and quickly converge toward near-zero values. After the transient phase, the errors remain consistently small across subsequent motion cycles. This indicates that the repetitive control mechanism successfully learns the periodic error pattern and effectively compensates for it in later iterations.

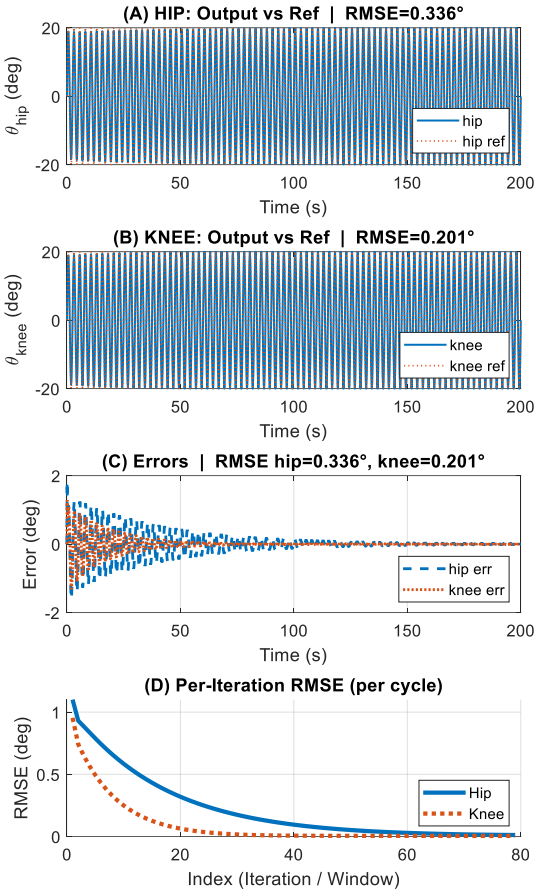

Fig. 9. Tracking at the optimal setting $L = 5$, rcLead $= 2$: (a) Hip: output vs ref; (b) Knee: output vs ref; (c) Errors per cycle; and (d) Per-iteration RMSE.

The per-iteration RMSE convergence presented in Fig. 9(d) provides additional evidence of the learning capability of the control framework. The RMSE decreases rapidly during the early iterations and gradually approaches a near-zero steady-state level as the number of repetitions increases. This convergence trend demonstrates that the combination of phase-lead compensation and FIR window-based filtering effectively enhances the error-learning dynamics of the repetitive control system.

The superior performance of the selected parameter combination can be explained by the balance it achieves between responsiveness and stability. The moderate window length (winLen = 5) provides sufficient smoothing of the learned error signal, improving noise tolerance without introducing excessive phase delay. At the same time, the moderate lead compensation (rcLead = 2) provides adequate phase advancement to improve transient response while maintaining system stability. Larger window lengths may introduce additional phase lag that slows convergence and increases steady-state error, whereas smaller windows may increase sensitivity to noise and produce oscillatory responses.

Overall, the results confirm that the configuration rcLead = 2 with winLen = 5 provides the most effective parameter setting for the proposed control strategy. This configuration achieves rapid convergence, minimal steady-state RMSE, and stable periodic tracking

performance for both hip and knee joints. The findings therefore demonstrate the suitability of the proposed control framework for high-precision trajectory tracking in robotic motion systems that require both fast adaptation and long-term stability.

V. Conclusion

This research presents a simulation-based analysis of a repetitive-control plug-in combined with a PID controller for a two-degree-of-freedom lower-limb robotic system. The control framework was implemented in a MATLAB environment with varying phase-lead compensation values and FIR Q-filter window lengths to evaluate cyclic trajectory tracking performance of the hip and knee joints. Tracking accuracy was evaluated using the RMSE across iterative learning cycles and under steady-state conditions. The results indicate that the repetitive-control structure significantly reduces periodic tracking errors and achieves stable convergence across successive learning cycles. Both joints exhibit rapid error reduction during the initial iterations, followed by consistent steady-state tracking performance. The parameter combination rcLead = 2 and winLen = 5 produced the best performance, yielding steady-state RMSE values of 0.014510 degrees for the hip joint and 0.004741 degrees for the knee joint. The analysis shows that moderate phase-lead compensation combined with an intermediate FIR window length provides a balanced trade-off between convergence speed, noise suppression, and control stability. In contrast, excessively short or long FIR windows increased noise sensitivity or introduced additional phase delay, while larger phase-lead values increased residual tracking errors. This paper provides a systematic analysis of the interaction between phase-lead compensation and FIR window length in repetitive control for cyclic robotic trajectory tracking. The findings offer practical guidance for selecting repetitive-control parameters in periodic robotic systems, particularly for wearable robotics and exoskeleton applications requiring stable cyclic motion. Although this study is limited to simulation analysis, it provides a foundation for future experimental validation. Future work will implement the proposed control architecture on a physical robotic platform and evaluate its performance under realistic actuator constraints, varying gait frequencies, and external disturbances.

Conflict of Interest

The authors declare no conflict of interest.

Author Contributions

Panya Minyong implemented the simulation framework, developed the repetitive-control algorithms, conducted the simulations, analyzed the experimental results, and prepared the initial manuscript draft; Phichitphon Chotikunnan conceived the research idea, designed the research methodology, supervised the overall study, provided technical guidance on repetitive control and exoskeleton-system modeling, validated the analytical results, revised the manuscript, and served as the corresponding author; Yutthana Pititheeraphab contributed to the control-system design, provided technical recommendations related to robotics and embedded systems, and assisted in validating the simulation results and control-performance analysis; Rawiphon Chotikunnan supported MATLAB implementation, figure preparation, and manuscript formatting; Nuntachai Thongpance provided recommendations related to biomedical engineering applications and reviewed the overall technical consistency of the study; Songtham Deewanichsakul contributed suggestions regarding mechatronic-system integration and control-system evaluation; Udomsak Jantontapo assisted in reviewing the simulation procedures and supporting the computational implementation; Surachat Chantarachit provided technical comments on dynamic-system modeling and interpretation of the control-performance results; all authors had approved the final version.

Acknowledgment

The researcher would like to thank the Research Institute, Academic Services Center, and College of Biomedical Engineering, Rangsit University for the grant of research funding to the research team. Furthermore, it is confirmed that the project has been reviewed by the Ethics Review Board of Rangsit University, with reference number RSUERB2025-006, which certifies that the research does not involve human subjects. Moreover, AI-driven methods (QuillBot Premium) were utilized for grammatical verification, paraphrasing, and linguistic augmentation to ensure the accuracy and clarity of the text.

References

[1] G. Masengo, X. Zhang, and R. Dong *et al.*, "Lower limb exoskeleton robot and its cooperative control: A review, trends, and challenges for future research," *Frontiers in Neurorobotics*, vol. 16, pp. 1–25, 2022. doi: 10.3389/fnbot.2022.913748

[2] S. Neťuková, M. Bejtic, and C. Malá *et al.*, "Lower limb exoskeleton sensors: State-of-the-art," *Sensors*, vol. 22, no. 23, no. 9091, 2022. doi: 10.3390/s22239091

[3] D. Shi, W. Zhang, and W. Zhang *et al.*, "A review on lower limb rehabilitation exoskeleton robots," *Chinese Journal of Mechanical Engineering*, vol. 32, no. 1, pp. 1–11, 2019.

[4] R. Baud, A. R. Manzoori, and A. Ijspeert *et al.*, "Review of control strategies for lower-limb exoskeletons to assist gait," *Journal of Neuro Engineering and Rehabilitation*, vol. 18, no. 119, 2021. doi: 10.1186/s12984-021-00906-3

[5] W. Z. Li, G. Z. Cao, and A. B. Zhu *et al.*, "Review on control strategies for lower limb rehabilitation exoskeletons," *IEEE Access*, vol. 9, pp. 123040–123060, 2021.

[6] J. Zhou, S. Yang, and Q. Xue, "Lower limb rehabilitation exoskeleton robot: A review," *Advances in Mechanical Engineering*, vol. 13, no. 4, pp. 1–17, 2021.

[7] R. Roy, M. Islam, and M. M. Rashid *et al.*, "Investigation of 2DOF PID controller for physiotherapeutic application for elbow rehabilitation," *Applied Sciences*, vol. 11, no. 18, 2021. doi: 10.3390/app11188617

[8] G. Bujgoi and D. Sendrescu, "Tuning of PID controllers using reinforcement learning for nonlinear system control," *Processes*, vol. 13, no. 3, art. no. 735, 2025. doi: 10.3390/pr13030735

[9] D. Zhou, Y. Yang, and X. Wu *et al.*, "Suppression of adverse effects of transmission clearance in brushless DC motor servo systems by switching compensation," in *Proc. Australian & New Zealand Control Conf. (ANZCC)*, 2024, pp. 131–136.

[10] Y. Liu and W. Sun, "High-performance position control for repetitive tasks of motor-driven servo systems based on periodic disturbance observer," *IEEE/ASME Trans. on Mechatronics*, vol. 28, no. 5, pp. 2461–2470, 2023.
[11] P. Shi, Y. Zhao, and J. Qin *et al.*, "Integrated adaptive repetitive learning control of linear motor servo systems with periodic tasks," *IEEE Trans. on Automation Science and Engineering*, vol. 22, pp. 21010–21019, Sep. 2025. doi: 10.1109/TASE.2025.3609458
[12] M. Steinbuch, "Repetitive control for systems with uncertain period-time," *Automatica*, vol. 38, no. 12, pp. 2103–2109, 2002. doi: 10.1016/S0005-1098(02)00134-6
[13] S. Mandra, A. Mystkowski, and H. Aschemann, "Robust design of a fractional-delay repetitive controller for uncertain feedback control systems and its validation on a magnetic bearing test rig," *IEEE Trans. on Control Systems Technology*, vol. 31, no. 6, pp. 2531–2542, 2023. doi: 10.1109/TCST.2023.3274923
[14] J. A. Prakosa, P. Purwowibowo, and E. Kurniawan *et al.*, "Discrete-time design of dual internal model-based repetitive control systems," *Applied Sciences*, vol. 12, no. 22, art. no. 11746, 2022. doi: 10.3390/app122211746
[15] G. Escobar, G. A. Catzin-Contreras, and M. J. Lopez-Sanchez, "Compensation of variable fractional delays in the 6k±1 repetitive controller," *IEEE Trans. on Industrial Electronics*, vol. 62, no. 10, pp. 6448–6456, 2015. doi: 10.1109/TIE.2015.2424202
[16] M. Nagahara and Y. Yamamoto, "Robust repetitive control by sampled-data H∞ filters," in *Proc. IEEE Conf. on Decision and Control (CDC) & Chinese Control Conf.*, 2009, pp. 8136−8141. doi: 10.1109/CDC.2009.5400156
[17] Z. Chen, X. Liang, and M. Zheng, "Deep iterative learning control for quadrotor's trajectory tracking," in *Proc. American Control Conf. (ACC)*, 2021, pp. 1408–1413. doi: 10.23919/ACC50511.2021.9483044
[18] S. Riaz, L. Hui, and M. S. Aldemir *et al.*, "A future concern of iterative learning control: A survey," *Journal of Statistics and Management Systems*, vol. 24, no. 6, pp. 1301–1322, 2021.
[19] Z. Zhuang, H. Tao, and Y. Chen *et al.*, "An optimal iterative learning control approach for linear systems with nonuniform trial lengths under input constraints," *IEEE Trans. on Systems, Man, and Cybernetics: Systems*, vol. 53, no. 6, pp. 3461–3473, 2023.
[20] C. Naveen, B. Meenakshipriya, and A. Tony Thomas *et al.*, "Real-time implementation of iterative learning control for an electro-hydraulic servo system," *IETE Journal of Research*, vol. 69, no. 2, pp. 649–664, 2023.
[21] X. Xu, P. Liu, and S. Lu *et al.*, "Iterative learning with adaptive sliding mode control for trajectory tracking of fast tool servo systems," *Applied Sciences*, vol. 14, no. 9, art. no. 3586, 2024. doi: 10.3390/app14093586
[22] Y. Chen, W. Jiang, and T. Charalambous, "Machine learning based iterative learning control for non-repetitive time-varying systems," *International Journal of Robust and Nonlinear Control*, vol. 33, no. 7, pp. 4098–4116, 2023.
[23] Z. Cao, Y. Feng, and X. Yu *et al.*, "Discrete-time sliding mode repetitive control for servo motor systems," *IEEE/ASME Trans. on Mechatronics*, vol. 30, no. 6, pp. 5444–5455, 2025.
[24] S. Massardi, D. Rodriguez-Cianca, and D. Pinto-Fernandez *et al.*, "Characterization and evaluation of human–exoskeleton interaction dynamics: A review," *Sensors*, vol. 22, no. 11, art. no. 3993, 2022. doi: 10.3390/s22113993
[25] J. Wu, S. Guo, and F. Yang *et al.*, "Research on an assist-as-needed gait correction control strategy based on admittance control," *Intelligent Service Robotics*, vol. 18, no. 3, pp. 567–578, 2025.
[26] X. Zhang, Y. Qu, and G. Zhang *et al.*, "Review of sEMG for exoskeleton robots: Motion intention recognition techniques and applications," *Sensors*, vol. 25, no. 8, no. 2448, 2025.
[27] M. Belal, N. Alsheikh, and A. Aljarah *et al.*, "Deep learning approaches for enhanced lower-limb exoskeleton control: A review," *IEEE Access*, vol. 12, pp. 143883–143907, 2024. doi: 10.1109/ACCESS.2024.3414175
[28] B. Huang, M. Zhai, and B. Lu *et al.*, "Gain-scheduled anti-windup PID control for LPV systems under actuator saturation and its application to aircraft," *Aerospace Systems*, vol. 5, no. 3, pp. 445–454, 2022. doi: 10.1007/s42401-022-00143-z
[29] L. Bergmann, O. Lueck, and D. Voss *et al.*, "Lower limb exoskeleton with compliant actuators: Design, modeling, and human torque estimation," *IEEE/ASME Trans. on Mechatronics*, vol. 28, no. 2, pp. 758–769, 2023. doi: 10.1109/TMECH.2022.3206530
[30] D. Rodriguez-Jorge, F. Romero-Sanchez, and D. R. Salgado *et al.*, "Transmission and actuation systems in cable-driven, walking-assistance exosuits based on postural and dynamic synergies," *Alexandria Engineering Journal*, vol. 77, pp. 383–393, 2023. doi: 10.1016/j.aej.2023.07.004
[31] Y. Li, X. Guan, and W. Li *et al.*, "Dynamic parameter identification of a human–exoskeleton system with the motor torque data," *IEEE Trans. on Medical Robotics and Bionics*, vol. 4, no. 1, pp. 206–218, 2021. doi: 10.1109/TMRB.2021.3137970
[32] H. Liao, H. H. T. Chan, and F. Gao *et al.*, "Proxy-based torque control of motor-driven exoskeletons for safe and compliant human–exoskeleton interaction," *Mechatronics*, vol. 88, art. no. 102906, 2022. doi: 10.1016/j.mechatronics.2022.102906
[33] S. Makarem, B. Delibas, and B. Koc, "Data-driven tuning of PID controlled piezoelectric ultrasonic motor," *Actuators*, vol. 10, no. 7, no. 148, 2021. doi: 10.3390/act10070148
[34] D. Pont-Esteban, M. Á. Sánchez-Urán, and M. Ferre, "Robust motion control architecture for an upper-limb rehabilitation exosuit," *IEEE Access*, vol. 10, pp. 113631–113648, 2022. doi: 10.1109/ACCESS.2022.3217528
[35] Y. Xing and W. Jiao, "Control method of lower limb rehabilitation robot based on nonlinear time series prediction model and sensor technology," *IEEE Access*, vol. 12, pp. 152532–152543, 2024. doi: 10.1109/ACCESS.2024.3480252
[36] F. Song, Y. Liu, and D. Shen *et al.*, "Learning control for motion coordination in wafer scanners: Toward gain adaptation," *IEEE Trans. on Industrial Electronics*, vol. 69, no. 12, pp. 13428–13438, 2022. doi: 10.1109/TIE.2022.3142428
[37] M. Tang, M. Di Benedetto, and S. Bifaretti *et al.*, "State of the art of repetitive control in power electronics and drive applications," *IEEE Open Journal of Industry Applications*, vol. 3, pp. 13–29, 2021. doi: 10.1109/OJIA.2021.3137589
[38] N. Li, Y. Yang, and G. Li *et al.*, "Multi-sensor fusion-based mirror adaptive assist-as-needed control strategy of a soft exoskeleton for upper limb rehabilitation," *IEEE Trans. on Automation Science and Engineering*, vol. 21, no. 1, pp. 475–487, 2024.
[39] T. Proietti, E. Ambrosini, and A. Pedrocchi *et al.*, "Wearable robotics for impaired upper-limb assistance and rehabilitation: State of the art and future perspectives," *IEEE Access*, vol. 10, pp. 106117–106134, 2022. doi: 10.1109/ACCESS.2022.3210514
[40] M. C. Lee, C. C. Chen, and C. T. Pan, "A multimodal sensor-integrated lower limb exoskeleton with digital twin framework for real-time gait rehabilitation," *IEEE Trans. on Instrumentation and Measurement*, vol. 75, 2026. doi: 10.1109/TIM.2026.3654715
[41] N. Schlüter, M. Neuhaus, and M. S. Darup, "Encrypted dynamic control with unlimited operating time via FIR filters," in *Proc. the European Control Conf. (ECC)*, 2021, pp. 952–957. doi: 10.23919/ECC54610.2021.9655161

Panya Minyong received the bachelor of industrial technology degree in industrial instrumentation technology from King Mongkut's Institute of Technology Ladkrabang, Thailand; the master of engineering degree in knowledge-based information and technology from Toyohashi University of Technology, Japan; and the doctor of engineering degree in information science and control from Toyohashi University of Technology, Japan. He is currently an associate professor in the Department of Mechatronics and Robotics Engineering, Faculty of Technical Education, Rajamangala University of Technology Thanyaburi, Thailand. His research interests include robotics, embedded systems, fuzzy logic control, and optimization.

Phichitphon Chotikunnan received the bachelor of engineering degree in mechatronics engineering from Pathumwan Institute of Technology, Thailand; the master of engineering degree in electrical engineering from King Mongkut's University of Technology Thonburi, Thailand; and the doctor of engineering degree in electrical and information engineering from King Mongkut's University of Technology Thonburi, Thailand. He is currently an associate professor in the Biomedical Engineering Program, College of Biomedical Engineering, Rangsit University, Thailand. His research interests include robotics, embedded systems, fuzzy logic control, and iterative learning control.

Rawiphon Chotikunnan bachelor of information technology degree in interactive design and game development from Dhurakij Pundit University, Thailand, and the Master of Engineering degree in biomedical engineering from Rangsit University, Thailand. He is currently a lecturer in the biomedical engineering program, College of Biomedical Engineering, Rangsit University, Thailand. His research interests include interactive media, medical image processing, robotics, and control systems.

Nuntachai Thongpance received the bachelor of science degree in physics from Prince of Songkla University, Thailand, in 1984, and the master of engineering degree in nuclear technology from Chulalongkorn University, Thailand, in 1987. He is currently an associate professor and dean of the College of Biomedical Engineering, Rangsit University, Thailand. His research interests include medical devices, biomedical engineering, and healthcare management engineering.

Yutthana Pititheeraphab is currently an assistant professor in the biomedical engineering program, College of Biomedical Engineering, Rangsit University, Thailand. He received the Doctor of Philosophy degree in biomedical engineering and the master of engineering degree in biomedical electronics engineering from King Mongkut's Institute of Technology Ladkrabang, Thailand. He obtained the bachelor of engineering degree in telecommunication technology from King Mongkut's Institute of Technology Ladkrabang, Thailand. His research interests include robotics, embedded systems, control systems, and image processing.

Songtham Deewanichsakul is currently an associate professor in the Faculty of Technical Education, Rajamangala University of Technology Thanyaburi, Thailand. He received his academic training in Mechanical Engineering. His research interests include mechanical engineering, mechatronics, PLC-based control systems, and engineering education.

Udomsak Jantontapo is currently an assistant professor in the Department of Mechatronics, Rajamangala University of Technology Thanyaburi, Thailand. He received the M.Sc. degree in computer science from the Asian Institute of Technology in 2006. He obtained the B.Sc. degree in Computer Science from Sripatum University in 2000. His research interests include computer programming, microcontroller applications, and vocational education.

Surachat Chantarachit is currently an assistant professor in the department of mechatronics, Rajamangala University of Technology Thanyaburi, Thailand. He received the doctor of engineering and master of engineering degrees in mechatronics from the Asian Institute of Technology in 2017 and 2011, respectively. He obtained the bachelor of engineering degree in mechatronics engineering from King Mongkut's University of Technology Thonburi in 2009. His research interests include dynamic systems, control, and mechanism design.